Ya.V. Karandas [1], A.V. Korotun [1, 2]

DIELECTRIC FUNCTION AND THE ABSORPTION CROSS-SECTION OF THE METAL-GRAPHENE NANOCYLINDERS OF THE FINITE LENGTH

[1] National University Zaporizhzhia Polytechnic
64 Zhukovskogo Str., Zaporizhzhia, 69063, Ukraine, E-mail: andko@zp.edu.ua
[2] G.V. Kurdyumov Institute for Metal Physics of National Academy of Sciences of Ukraine
36 Academician Vernadsky Blvd., Kyiv, 03142, Ukraine

The behavior of the diagonal components of the dielectric tensor and the behavior of the absorption cross-section in the different frequency ranges for the composite cylindrical nanostructures "metallic core – graphene shell" have been studied. In order to obtain the calculation formulas one uses the relations for the longitudinal and transverse components of the dielectric tensors for metallic core and graphene shell, which are determined by Drude model and Cubo model correspondingly. The consideration is carried out in the frameworks of "equivalent" elongated spheroid approach, according to which the defining dimensional parameter is effective aspect ratio, calculated from the condition of the equality of the corresponding axial inertia moments for two-layer cylinder and the "equivalent" elongated spheroid. The numerical results have been obtained for the nanocylinders with the cores of different metals, different radius and with the different number of graphene layers. The variation of amplitude and the variation of the location of extremes of the real and imaginary parts of the transverse component of the dielectric tensor under the increase in radius of the metallic core and the thickness of the graphene shell have been analyzed. It has been shown that the variation of the radius of the core has the significantly greater influence on the properties of the polarizability resonances and absorption cross-section than the variation of the number of graphene layers. The reasons of the presence of two maxima of the absorption cross-section for the metal-graphene cylinders which differ in both amplitude and width and located in infrared, violet and near ultraviolet parts of the spectrum and their relation with the surface plasmonic resonances in the metallic core and with the terahertz plasmons of graphene have been found. The factors which have an effect on amplitude and on the shift of the maxima of the absorption cross-section have been found. The reasons of the different width of maxima, which are located in the different spectral intervals, have been determined.

Keywords: *metal-graphene nanocylinder, dielectric tensor, relaxation rate, absorption cross-section, depolarization factor, equivalent ellipsoid, effective aspect ratio*

INTRODUCTION

An intensive study of the metallic nanostructures in the recent two decades is associated with their unique electronic, optical and magnetic properties which differ from the similar properties of bulk substance [1–3]. The majority of these differences are conditioned by the large ratio of the surface area to volume and by the spatial limitations of the electron motion.

One of the most important factors, which determines the optical properties of the nanostructures, is their shape. Thus, the non-spherical metallic nanostructures demonstrate anisotropic optical and electronic responses, which are determined by their topological particularities [4–7]. Among the various nonspherical nanostructures nano-cylinders receive much attention. This is due to, from one

hand, improvement in the technologies of their synthesis [8–12], and, from the other hand, broad prospects of the application in photonics, electronics, catalysis and medicine [8, 9, 13–17].

It is known that the use of metallic nanostructures for the localization of the electromagnetic field in the domain, the sizes of which are less than the diffraction limit, has limitations in the mid-IR range. Moreover, the recent studies show that the photothermal stability of the metallic nanoparticles, as the necessary particularity of the photothermal cancer therapy, decreases under the long-term laser exposure [18]. In order to solve these problems one proposes to use the stable shells, for example, polymeric ones [19, 20], to preserve the surface structure of the nanoparticles. Despite the fact that such coatings reduce the unwanted effect on the body, in

practice it is rather difficult to control their thickness. An alternative approach to this problem consists in the use of graphene, which poses the suitable for the biomedical applications properties [16, 21, 22]. Thus, graphene, along with the low toxicity and the large ratio of the surface area to volume, has the high functionalization rate, which can contribute to the strong interaction with the biological tissues and high permeability of the nanoparticles into the tumor tissues [23]. Apart from this, graphene with the adjustable thickness (number of layers) is chemically inert and has the perfect chemical stability in the physiological solutions [23], and the thermal stability of golden nanoparticles, covered with graphene layer, increases under the long-term laser exposure [24]. Moreover the peak of the localized surface plasmonic resonance of the metal-graphene nanocylinders can be easily adjusted inside the biological transparency area, controlling both the geometrical sizes of the metallic core and the thickness of graphene layers and the aspect ratio [25, 26]. Due to this fact the nanocylinders, covered with graphene, has the great efficiency as the photothermal therapy agents. Most of the works (see, for example, [25, 26]) do not take into account the influence of the size effects, the surface scattering and the radiation attenuation on the behavior of plasmons under the study of the optical properties of metal-graphene nanoparticles.

Let us point out that the strict theory of the size effects and their influence on the characteristics of plasmons in the metallic spheroidal nanoparticles has been developed in the works [27–31] adapted for the case of the metallic nanodiscs and nanorods, two-layer spherical and cylindrical nanostructures in the works [32–37]. Hence, the aim of this work is the study of the optical properties of metal-graphene nanocylinders in the frameworks of the kinetic approach to the calculation of the surface scattering and the radiation attenuation rates.

BASIC RELATIONS

Let us consider metal-graphene 1D-structure with the thickness of graphene shell t ($t = Nt_G = b-a$, where N is the number of graphene layers; $t_G = 0.335$ nm is the thickness of monoatomic graphene layer; a is the radius of metallic core; b is total radius of the nanocylinder), placed into the medium with the

dielectric permittivity ϵ_m (Fig. 1). Due to anisotropy of the considered composite nanostructure its dielectric permittivity is the diagonal second rank tensor

$$\epsilon_@ = \begin{pmatrix} \epsilon_@^\perp & 0 & 0 \\ 0 & \epsilon_@^\perp & 0 \\ 0 & 0 & \epsilon_@^\| \end{pmatrix}, \tag{1}$$

where the expressions for the components $\epsilon_@^{\perp(\|)}$ in the frameworks of the "equivalent" spheroid approach, proposed by the authors, coincide with the relations for two-layer elongated ellipsoid of revolution [38]

$$\epsilon_@^{\perp(\|)} = \epsilon_G^{\perp(\|)} + \beta_c \frac{\epsilon_G^{\perp(\|)}\left(\epsilon_c^{\perp(\|)} - \epsilon_G^{\perp(\|)}\right)}{\epsilon_G^{\perp(\|)} + \left(\epsilon_c^{\perp(\|)} - \epsilon_G^{\perp(\|)}\right)\left(\mathcal{L}_{\perp(\|)}^{(1)} - \beta_c\mathcal{L}_{\perp(\|)}^{(2)}\right)}. \tag{2}$$

Here $\epsilon_c^{\perp(\|)}$ and $\epsilon_G^{\perp(\|)}$ are transverse (longitudinal) components of dielectric permittivity of core and shell materials, correspondingly; $\mathcal{L}_{\perp(\|)}^{(1)}$ and $\mathcal{L}_{\perp(\|)}^{(2)}$ are transverse (longitudinal) depolarization coefficients of the internal and external layers; $\beta_c = V_c / V$, V_c is the volume of the internal ellipsoid, V is the total volume of ellipsoids.

Let us determine the depolarization factors $\mathcal{L}_{\perp(\|)}^{(1)}$ and $\mathcal{L}_{\perp(\|)}^{(2)}$ from the corresponding relations for the prolate spheroids

$$\mathcal{L}_\|^{(1,2)} = \frac{\varrho_{eff}^{(1,2)2}}{2\left(1-\varrho_{eff}^2\right)^{\frac{3}{2}}}\left(\ln\frac{1+\sqrt{1-\varrho_{eff}^{(1,2)2}}}{1-\sqrt{1-\varrho_{eff}^{(1,2)2}}} - 2\sqrt{1-\varrho_{eff}^{(1,2)2}}\right),$$

$$\mathcal{L}_\perp^{(1,2)} = \frac{1}{2}\left(1-\mathcal{L}_\|^{(1,2)}\right), \tag{3}$$

where $\varrho_{eff}^{(1,2)}$ is effective aspect ratios

$$\varrho_{eff}^{(1,2)} = \frac{2\varrho^{(1,2)}}{\sqrt{3}}, \qquad \varrho^{(1,2)} = \frac{2r^{(1,2)}}{l}, \tag{4}$$

and l – the length of the cylinder, $r^{(1)} = a$ and $r^{(2)} = b$ – the radius of the metallic core and of the entire 1D-particle correspondingly.

Let us point out that the expression for the effective aspect ratio can be obtained from the condition of the equality of the corresponding

axial moments of inertia for the cylinder and the "equivalent" elongated spheroid [39].
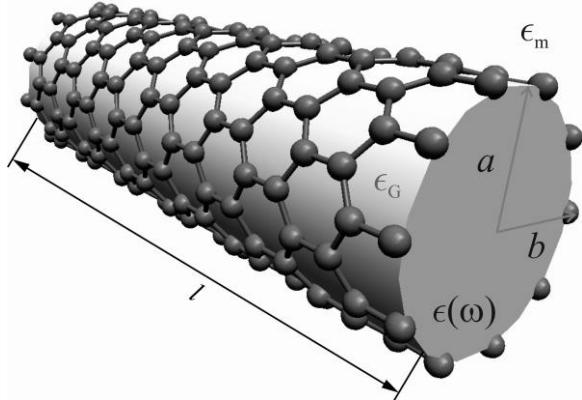
Fig. 1. Geometry of the problem

According to Drude theory the components of the dielectric tensor of metallic core are determined by the following expressions

$$\epsilon_c^{\perp(\parallel)}(\omega) = \epsilon^\infty - \frac{\omega_p^2}{\omega^2 + \left(\gamma_{eff}^{\perp(\parallel)}\right)^2} + i\frac{\omega_p^2 \gamma_{eff}^{\perp(\parallel)}}{\omega\left(\omega^2 + \left(\gamma_{eff}^{\perp(\parallel)}\right)^2\right)}, \quad (5)$$

where ϵ^∞ is the contribution of ion core into the dielectric function of metal; $\omega_p = \sqrt{e^2 n_e / \epsilon_0 m^*}$ is the frequency of bulk plasmons, e, n_e and m^* are charge, concentration and the effective mass of electron ($n_e^{-1} = 4\pi r_s^3 / 3$, r_s is mean distance between conductivity electrons), the effective relaxation rate [28]

$$\gamma_{eff}^{\perp(\parallel)} = \gamma_{bulk} + \gamma_s^{\perp(\parallel)} + \gamma_{rad}^{\perp(\parallel)}. \quad (6)$$

In formula (7) γ_{bulk} is bulk relaxation rate, $\gamma_s^{\perp(\parallel)}$ and $\gamma_{rad}^{\perp(\parallel)}$ are transverse (longitudinal) relaxation rates, associated with the scattering on the surface and with the radiation attenuation and determined by the relations [27–31]

$$\gamma_s^{\perp(\parallel)} = \frac{\mathcal{L}_{\perp(\parallel)}^{(1)} \sigma_{\perp(\parallel)}}{\epsilon_0\left[\epsilon_m + \mathcal{L}_{\perp(\parallel)}^{(1)}(1 - \epsilon_m)\right]}; \quad (7)$$

$$\gamma_{rad}^{\perp(\parallel)} = \frac{2V}{9\pi\epsilon_0}\left(\frac{\omega_p}{c}\right)^3 \frac{\mathcal{L}_{\perp(\parallel)}^{(1)} \sigma_{\perp(\parallel)}}{\sqrt{\epsilon_m\left[\epsilon^\infty + \left(\frac{1}{\mathcal{L}_{\perp(\parallel)}^{(1)}} - 1\right)\epsilon_m\right]}}, \quad (8)$$

where c – light velocity, and the diagonal components of the conductivity tensor have the form

$$\sigma_{\perp(\parallel)} = \frac{9}{16}\epsilon_0\left(\frac{\omega_p}{\omega}\right)^2 v_{s,\perp} \mathscr{F}_{\perp(\parallel)}\left(\varrho_{eff}^{(1)}\right); \quad (9)$$

v_F – Fermi electron velocity, and the expressions for $\mathscr{F}_{\perp(\parallel)}\left(\varrho_{eff}^{(1)}\right)$ have the form similar to:

$$\mathscr{F}_\perp\left(\varrho_{eff}^{(1)}\right) = \left(1 - \varrho_{eff}^{(1)2}\right)^{-\frac{3}{2}}\left\{\varrho_{eff}^{(1)}\left(\frac{3}{2} - \varrho_{eff}^{(1)2}\right)\sqrt{1 - \varrho_{eff}^{(1)2}} + \right.$$
$$\left. + \left(\frac{3}{4} - \varrho_{eff}^{(1)2}\right)\ln\left(\varrho_{eff}^{(1)} + \sqrt{1 - \varrho_{eff}^{(1)2}}\right)\right\}; \quad (10)$$

$$\mathscr{F}_\parallel\left(\varrho_{eff}^{(1)}\right) = \left(1 - \varrho_{eff}^{(1)2}\right)^{-\frac{3}{2}}\left\{\frac{\pi}{2} - \arcsin\varrho_{eff}^{(1)} + \right.$$
$$\left. + \varrho_{eff}^{(1)}\left(1 - 2\varrho_{eff}^{(1)2}\right)\sqrt{1 - \varrho_{eff}^{(1)2}}\right\}. \quad (11)$$

One can write down the following for the real and imaginary parts of the components of the dielectric permittivity tensor for the graphene layer [40]

$$\text{Re}\,\epsilon_G^\perp = 2.5, \quad \text{Im}\,\epsilon_G^\perp = 0;$$

$$\text{Re}\,\epsilon_G^\parallel(\omega) = \text{Re}\,\epsilon_G^\perp - \frac{\text{Im}\,\sigma_G(\omega)}{\epsilon_0 \omega t},$$

$$\text{Im}\,\epsilon_G^\parallel(\omega) = \frac{\text{Re}\,\sigma_G(\omega)}{\epsilon_0 \omega t}, \quad (12)$$

where the permittivity of graphene is determined by the sum of contributions from intraband and interband transitions according to Cubo theory [40]

$$\sigma_G(\omega) = \sigma_{intra}(\omega) + \sigma_{inter}(\omega); \quad (13)$$

and

$$\sigma_{intra}(\omega) = \frac{i e^2 k_B T}{\pi\hbar^2(\omega + i\gamma_G)}\left\{\frac{\mu_c}{k_B T} + 2\ln\left(e^{-\frac{\mu_c}{k_B T}} + 1\right)\right\};$$

$$\sigma_{inter}(\omega) = \frac{i e^2}{4\pi\hbar^2}\ln\frac{2|\mu_c| - \hbar(\omega + i\gamma_G)}{2|\mu_c| + \hbar(\omega + i\gamma_G)}, \quad (14)$$

or, separating the real part from the imaginary part,

$$\text{Re}\,\sigma_{intra}(\omega) = \frac{e^2 k_B T\gamma_G}{\pi\hbar^2(\omega^2 + \gamma_G^2)}\left\{\frac{\mu_c}{k_B T} + 2\ln\left(e^{-\frac{\mu_c}{k_B T}} + 1\right)\right\};$$

$$\text{Im}\,\sigma_{\text{intra}}\left(\omega\right)=\frac{e^2 k_{\text{B}} T \omega}{\pi \hbar^2 \left(\omega^2+\gamma_{\text{G}}^2\right)}\left\{\frac{\mu_{\text{c}}}{k_{\text{B}} T}+2\ln\left(e^{-\frac{\mu_{\text{c}}}{k_{\text{B}} T}}+1\right)\right\};$$

(15)

$$\text{Re}\,\sigma_{\text{inter}}\left(\omega\right)=\frac{e^2}{4\pi \hbar^2}\,\text{arctg}\,\frac{4\left|\mu_c\right|\hbar\gamma_{\text{G}}}{4\left|\mu_c\right|^2-\hbar^2\left(\omega^2+\gamma_{\text{G}}^2\right)}$$

$$\text{Im}\,\sigma_{\text{inter}}\left(\omega\right)=\frac{e^2}{4\pi \hbar^2}\ln\frac{\sqrt{16\left|\mu_c\right|^4+\hbar^4\left(\omega^2+\gamma_{\text{G}}^2\right)^2-8\left|\mu_c\right|^2\hbar^2\left(\omega^2-\gamma_{\text{G}}^2\right)}}{\left(2\left|\mu_c\right|+\hbar\omega\right)^2+\hbar^2\gamma_{\text{G}}^2}.$$

(16)

$$C_{@}^{\text{abs}}=\frac{\omega}{c}\frac{V}{3}\epsilon_{\text{m}}^{3/2}\left\{2\frac{\left(1/\mathcal{L}_{\perp}^{(2)}\right)^2\text{Im}\,\epsilon_{@}^{\perp}}{\left(\text{Re}\,\epsilon_{@}^{\perp}+\frac{1-\mathcal{L}_{\perp}^{(2)}}{\mathcal{L}_{\perp}^{(2)}}\epsilon_{\text{m}}\right)^2+\left(\text{Im}\,\epsilon_{@}^{\perp}\right)^2}+\frac{\left(1/\mathcal{L}_{\parallel}^{(2)}\right)^2\text{Im}\,\epsilon_{@}^{\parallel}}{\left(\text{Re}\,\epsilon_{@}^{\parallel}+\frac{1-\mathcal{L}_{\parallel}^{(2)}}{\mathcal{L}_{\parallel}^{(2)}}\epsilon_{\text{m}}\right)^2+\left(\text{Im}\,\epsilon_{@}^{\parallel}\right)^2}\right\}.$$

(17)

In formulas (14)–(16): μ_c – the chemical potential (Fermi energy) in graphene, γ_G – electron relaxation rate in graphene.

Knowing the dielectric function of metal-graphene cylinder, one can calculate such observable value as the absorption cross-section $C_{@}^{\text{abs}}$. Thus, according to Gans [41, 42], one can wright down

The formulas (2) and (17) taking into account the relations (3)–(16) are used further in order to obtain the numerical results.

THE RESULTS OF CALCULATIONS AND DISCUSSION

The calculations have been performed for the composite cylinders with the core of different metals. The parameters of metals, graphene and the matrix are given in Tables 1 and 2, respectively.

The Fig. 2 shows the frequency dependences for the real and imaginary parts of the transverse component of the dielectric tensor for the nanocylinders $\text{Ag}@\text{G}$ of the different sizes. The results of the calculations show the qualitative similarity of the curves $\text{Re}\,\epsilon_{@}^{\perp}\left(\omega\right)$ (Fig. 2 *a*) for the considered structures with metallic core of the different radius, which consist in the presence of maximum and minimum on the curves, the sign-variability of the frequency dependences for the real part of the transverse component of the dielectric tensor. It should be pointed out that the greater the radius of the metallic core is, under the same thickness of the graphene shell, the less expressed the maxima $\max\left[\text{Re}\,\epsilon_{@}^{\perp}\left(\omega\right)\right]$ is with the simultaneous shift of the maxima into the lower frequency range. The maxima $\text{Im}\,\epsilon_{@}^{\perp}\left(\omega\right)$ behave in the similar way (Fig. 2 *b*), and, apart from this, the increase in their width due to the increase in the radiation attenuation rate with the increase in the radius of the metallic core takes place.

Table 1. Parameters of metals (for example, [7] and the references there)

Metal	Parameter				
	Z	r_s/a_0	m^*/m_e	ϵ^{∞}	$\gamma_{\text{bulk}}, 10^{14}\ \text{s}^{-1}$
Al	3	2.11	1.06	0.7	1.25
Cu	1	2.67	1.49	12.03	0.37
	2	2.11			
Au	1	3.01	0.99	9.84	0.35
	3	2.09			
Ag	1	3.02	0.96	3.7	0.25

Table 2. Parameters of the shell and matrix (for example, [6] and references there in)

	Shell graphene		Matrix teflon
μ_c, eV		γ_G, 10^{12} s^{-1}	ϵ_m
0.1		6.67	2.3

Fig. 3 shows the frequency dependences for the absorption cross-sections of the cylinders Ag@G with the different sizes of the core and with the different number of graphene layers. It should be pointed out that the increase in the radius of the metallic core (under the constant number of graphene layers) results in the increase in amplitude of the maxima and in their "blue" shift. At the same time, if the increase in amplitude and the frequency shift of the first maximum are significant, then, as for the second maximum, these values are significantly less. Apart from this, the width of the first resonances is significantly less than the width of the second ones. Such behavior of the dependences $C_@^{abs}(\omega)$ can be explained as follows: the strongly expressed maxima of the small width are the manifestation of the optical properties of graphene layers and the longitudinal plasmonic resonance of silver core in the red and infrared parts of the spectrum, and the weakly expressed maxima of the large width in the near ultraviolet range correspond to the transverse plasmonic resonance of the metallic core. This explanation is confirmed by the curves of the frequency dependence for the absorption cross-section with the different number of graphene layers with the fixed radius of the core (Fig. 3 *b*). One can see that the increase in the number of the layers results in only the slight decrease in amplitude of the resonances, and moreover, their spectral location remains the same. The different width of the resonances is explained by the fact that $\gamma_{eff}^{\parallel} \ll \gamma_{eff}^{\perp}$ and by the small value of the electron relaxation rate in graphene.

Fig. 4 shows the frequency dependences for the absorption cross-sections for Me@G cylinders with the core of different metals. Let us point out that the variation of metal of the core results in the significant shift of the second maximum, while the shift of the first maximum is insignificant. It is also indicates that the properties of the second maximum are determined exceptionally by the characteristics of metal, while the plasmons of graphene layers have an effect on the properties of the first maximum.

The frequency dependences for the absorption cross-section of the nanocylinders Au@G and Cu@G in the cases of different valence of metal atoms (Fig 4 *b*) indicate that the valence variation also has the significant effect on the location of the second maximum and has the insignificant effect on the location of the first maximum. The similar effect also takes place in the case of the different effective masses of electrons, illustrated by the example of the nanocylinders Al@G (Fig. 4 *c*).
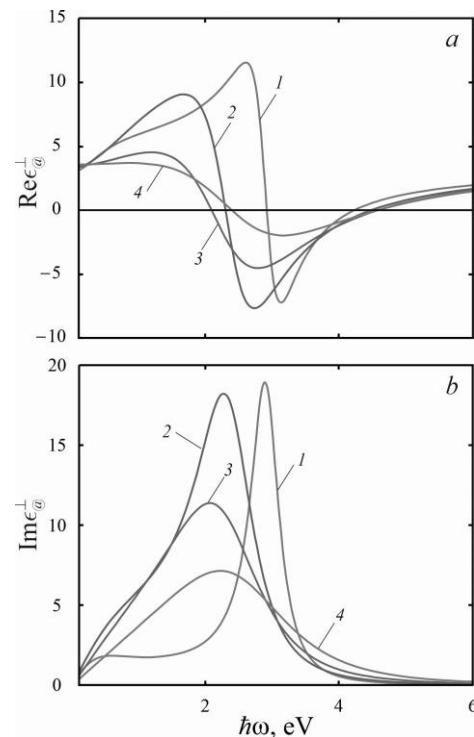
Fig. 2. The frequency dependences for the real (*a*) and imaginary (*b*) parts of the transverse component of the dielectric tensor for the nanocylinders Ag@G with the different radius of the metallic core and the number of graphene layers $N = 15$: *1* – $R_c = 10$ nm; *2* – $R_c = 25$ nm; *3* – $R_c = 50$ nm; *4* – $R_c = 100$ nm
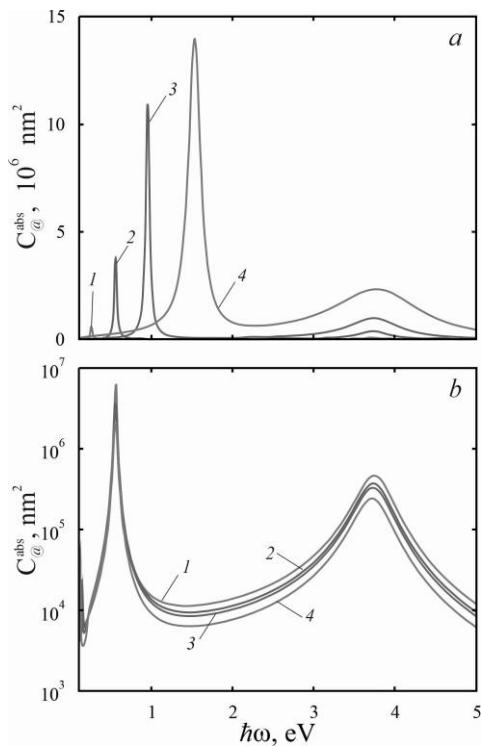
Fig. 3. The frequency dependences for the absorption cross-sections for the nanocylinders $\mathrm{Ag@G}$ under the fixed number of graphene layers ($N = 15$) and the same values of the core radiuses as in Fig 2 *a* and with the fixed core radius ($R_c = 25$ nm) under the different number of graphene layers (*b*): *1* – $N = 1$; *2* – $N = 10$; *3* – $N = 15$; *4* – $N = 30$

CONCLUSIONS

The relations for the frequency dependences for the diagonal components of the dielectric tensor and the relations for the frequency dependences for the absorption cross-section of metal-graphene nanocylinders of the finite length have been obtained using the "equivalent" spheroid approach.

It has been shown that the increase in the radius of the metallic core under the same thickness of graphene shell results in the decrease in amplitude of the extremes of the real and imaginary parts of the transverse component of the dielectric tensor, and also in the "red" shift of the extremes for the nanocylinders $\mathrm{Ag@G}$.

It has been found that the frequency dependences for the absorption cross-section have two maxima. At the same time, the strongly expressed maxima of the small width are situated in the infrared and red parts of the spectrum (in the biological window of transparency) and

associated with the excitation of plasmons in graphene layers and with the excitation of the surface plasmonic resonances in silver core. The weakly expressed wide maxima in the near ultraviolet domain are caused by the excitation of the transverse surface plasmonic resonance.
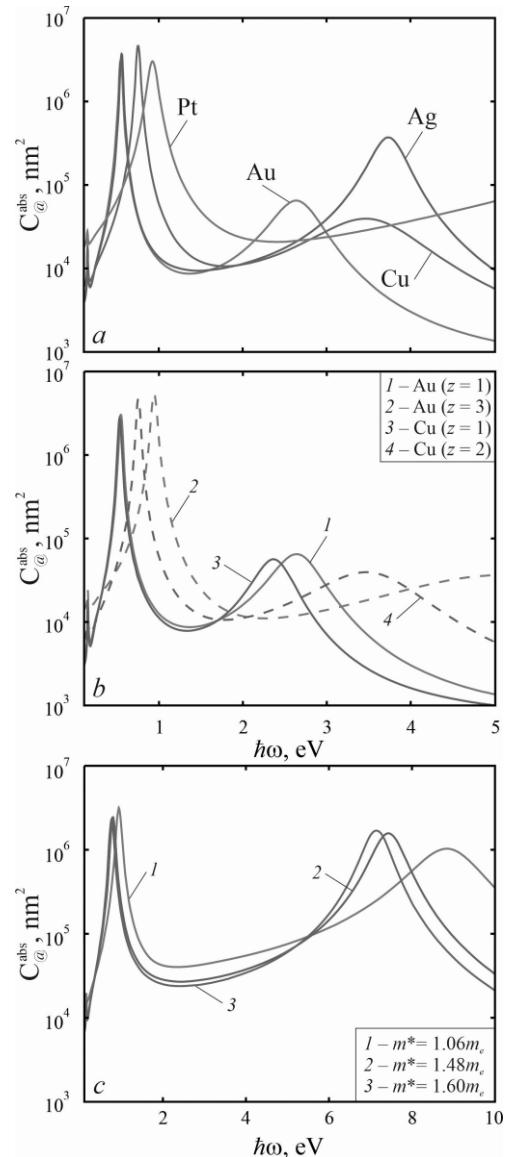
Fig. 4. The frequency dependences for the absorption cross-section for the nanocylinders Me@G under $R_c = 25$ nm, $N = 10$ for the cases: cores, produced of different metals (*a*); cores, produced of gold and copper with atoms of different valence (*b*); cores, produced of aluminum under the different values of effective mass of electrons (*c*)

The presence of the maxima of the absorption cross-section in the biological window of transparency indicates the appropriateness of the use of metal-graphene nanocylinders as the cancer phototherapy agents.

The different width of the maxima of the absorption cross-section is explained by the low electron relaxation rate in graphene and by the fact that the longitudinal components of the tensor of the effective electron relaxation rate in metal are significantly less than transverse components.

It has been demonstrated that the variation of metal of the core, the valence of atoms of core metal, and also the variation of the value of the effective mass of electron result in the significant shift of the weakly expressed maxima. At the same time, the mentioned factors have the insignificant effect on the shift of the maxima, caused by the transverse surface plasmonic resonance.

Діелектрична функція і переріз поглинання метал-графенових наноциліндрів скінченої довжини

Я.В. Карандась, А.В. Коротун

Національний університет «Запорізька політехніка»
вул. Жуковського, 64, Запоріжжя, 69063, Україна, andko@zp.edu.ua
Інститут металофізики ім. Г.В. Курдюмова Національної академії наук України
бульвар Академіка Вернадського, 36, Київ, 03142, Україна

В роботі досліджено поведінку діагональних компонентів діелектричного тензора і перерізу поглинання у різних частотних діапазонах для композитних циліндричних наноструктур «металева серцевина – графенова оболонка». З метою отримання розрахункових формул використовуються співвідношення для поздовжніх та поперечних компонентів діелектричних тензорів металевого осердя і графенової оболонки, що визначаються моделями Друде і Кубо, відповідно. Розгляд проводиться у рамках підходу «еквівалентного» витягнутого сфероїда, згідно з яким визначальним розмірним параметром є ефективне аспектне відношення, що обчислюється з умови рівності відповідних осьових моментів інерції двошарового циліндра та «еквівалентного» витягнутого сфероїда. Чисельні результати отримані для наноциліндрів із сердечниками різних металів, різного радіуса та з різним числом графенових шарів. Проаналізовано зміни амплітуд і положень екстремумів дійсної та уявної частин поперечної компоненти діелектричного тензора зі збільшенням радіуса металевого осердя і товщини графенової оболонки. Показано, що на властивості резонансів поляризовності і перерізу поглинання зміна радіуса осердя впливає більш істотно, ніж зміна кількості графенових шарів. Встановлено причини наявності двох максимумів перерізів поглинання метал-графенових циліндрів, що відрізняються як амплітудою, так і шириною, і розташовуються в інфрачервоній, фіолетовій та ближній ультрафіолетовій областях спектра, а також їхній зв'язок із поверхневими плазмонними резонансами у металевому осерді і терагерцевими плазмонами. Визначено фактори, що впливають на амплітуду та зміщення максимумів перерізу поглинання. З'ясовано причини різної ширини максимумів, що знаходяться у різних спектральних інтервалах.

Ключові слова: метал-графеновий наноциліндр, діелектричний тензор, швидкість релаксації, переріз поглинання, фактор деполяризації, еквівалентний еліпсоїд, ефективне аспектне відношення

REFERENCES

1. Dmitruk N.L., Goncharenko A.V., Venger E.F. *Optics of small particles and composite media*. (Kyiv: Naukova Dumka, 2009).
2. Schasfoort R.B.M. *Handbook of Surface Plasmon Resonance:* Edition 2. (Royal Society of Chemistry, 2017).

_____

3. Korotun A.V., Koval' A.O., Kryuchin A.A., Rubish V.M., Petrov V.V., Titov I.M. *Nanophoton technologies. Modern state and prospects*. (Uzhgorod: PE Sabov A.M., 2019). [in Ukrainian].

4. Sau T.K., Rogach A.L., Jäckel F., Klar T.A., Feldmann J. Properties and applications of colloidal nonspherical noble metal nanoparticles. *Adv. Mater.* 2010. **22**(16): 1805.

5. Grigorchuk N.I. Plasmon resonant light scattering on spheroidal metallic nanoparticle embedded in a dielectric matrix. *Europhys. Lett.* 2012. **97**(4): 45001.

6. Karandas Ya., Korotun A. An optical radiation efficiency of the composite nanocylinders. In: *International Conference on Electronics and Information Technologies (ELIT 2021)*. Proc. 12th Int. Conf. (May, 2021, Lviv, Ukraine). P. 222.

7. Korotun A.V., Pavlyshche N.I. Cross Sections for Absorption and Scattering of Electromagnetic Radiation by Ensembles of Metal Nanoparticles of Different Shapes. *Phys. Met. Metall.* 2021. **122**(10): 941.

8. Huang X.H., Neretina S., El-Sayed M.A. Gold Nanorods: From Synthesis and Properties to Biological and Biomedical Applications. *Adv. Mater.* 2009. **21**(48): 4880.

9. Pérez-Juste J., Pastoriza-Santos I., Liz-Marzán L.M., Mulvaney P. Gold nanorods: Synthesis, characterization and applications. *Coord. Chem. Rev.* 2005. **249**(17–18): 1870.

10. Gole A., Murphy C.J. Seed-Mediated Synthesis of Gold Nanorods: Role of the Size and Nature of the Seed. *Chem. Mater.* 2004. **16**(19): 3633.

11. Nikoobakht B., El-Sayed M.A. Preparation and Growth Mechanism of Gold Nanorods (NRs) Using Seed-Mediated Growth Method. *Chem. Mater.* 2003. **15**(10): 1957.

12. Busbee B.D., Obare S.O., Murphy C.J. An Improved Synthesis of High-Aspect-Ratio Gold Nanorods. *Adv. Mater.* 2003. **15**(5): 414.

13. Fu G., Liu W., Feng S., Yue X. Prussian blue nanoparticles operate as a new generation of photothermal ablation agents for cancer therapy. *Chem. Commun.* 2012. **48**(94): 11567.

14. Wei H., Pan D., Zhang S., Li Z., Li Q., Liu N., Wang W., Xu H. Plasmon Waveguiding in Nanowires. *Chem. Rev.* 2018. **118**(6): 2882.

15. Khan N.U., Lin J., Younas M.R., Liu X., Shen L. Synthesis of gold nanorods and their performance in the field of cancer cell imaging and photothermal therapy. *Cancer Nanotechnol.* 2021. **12**(1): 20.

16. Zhang M., Zhang X., Zhao K., Dong Y., Yang W., Liu J., Li D. Assembly of gold nanorods with L-cysteine reduced graphene oxide for highly efficient NIR-triggered photothermal therapy. *Spectrochim. Acta A: Molec. Biomol. Spectrosc.* 2022. **266**: 120458.

17. Ding S., Ma L., Feng J., Chen Y., Yang D., Wang Q. Surface-roughness-adjustable Au nanorods with strong plasmon absorption and abundant hotspots for improved SERS and photothermal performances. *Nano Research*. 2022. **15**(3): 2715.

18. Sun J., Yu X., Li Z., Zhao J., Zhu P., Dong X., Yu Z., Zhao Z., Shi D., Wang J., Dai H. Ultrasonic Modification of Ag Nanowires and Their Applications in Flexible Transparent Film Heaters and SERS Detectors. *Materials*. 2019. **12**(6): 893.

19. Zhang Y., Xu D., Li W., Yu J., Chen Y. Effect of Size, shape, and surface modification on cytotoxicity of gold nanoparticles to human HEp-2 and canine MDCK cells. *J. Nanomater.* 2012. **2012**(7): 7.

20. Rayavarapu R.G., Petersen W., Hartsuiker L., Chin P., Janssen H., Van Leeuwen F.W.B., Otto C., Manohar S., Van Leeuwen T.G. In vitro toxicity studies of polymer-coated gold nanorods. *Nanotechnology*. 2010. **21**(14): 145101.

21. Feng L., Liu Z. Graphene in biomedicine: opportunities and challenges. *Nanomedicine*. 2011. **6**(2): 317.

22. Fares H., Almokhtar M., Almarashi J.Q.M., Rashad M., Moustafa S. Tunable narrow-linewidth surface plasmon resonances of graphene-wrapped dielectric nanoparticles in the visible and near-infrared. *Physica E*. 2022. **142**: 115300.

23. Markovic Z.M., Harhaji-Trajkovic L.M., Todorovic-Markovic B.M., Kepić D.P., Arsikin K.M., Jovanović S.P., Pantovic A.C., Dramićanin M.D., Trajkovic V.S. In vitro comparison of the photothermal anticancer activity of graphene nanoparticles and carbon nanotubes. *Biomaterials*. 2011. **32**(4): 1121.

24. Bian X., Song Z.L., Qian Y., Gao W., Cheng Z.Q., Chen L., Liang H., Ding D., Nie X.K., Chen Z., Tan W. Fabrication of graphene-isolated-Au-nanocrystal nanostructures for multimodal cell imaging and photothermal-enhanced chemotherapy. *Sci. Rep.* 2014. **4**: 6093.

25. Farokhnezhad M., Esmaeilzadeh M. Graphene coated gold nanoparticles: an emerging class of nanoagents for photothermal therapy applications. *Phys. Chem. Chem. Phys.* 2019. **21**(33): 18352.

26. Farokhnezhad M., Esmaeilzadeh M., Nourian M., Jalaeikhoo H., Rajaeinejad M., Iravani S., Majidzadeh-A K. Silica-gold nanoshell@graphene: A novel class of plasmonic nanoagents for photothermal cancer therapy. J. Phys. D: Appl. Phys. 2020. **53**(40): 405401.

27. Grigorchuk N.I., Tomchuk P.M. Optical and transport properties of spheroidal metal nanoparticles with account for the surface effect. *Phys. Rev. B*. 2011. **84**(8): 085448.

28. Grigorchuk N.I. Radiative damping of surface plasmon resonance in spheroidal metallic nanoparticle embedded in a dielectric medium. *J. Opt. Soc. Am. B*. 2012. **29**(12): 3404.

29. Tomchuk P.M. Dependence of light scattering cross-section by metal nanoparticles on their shape. *Ukr. Fiz. Zh.* 2012. **57**: 553. [in Ukrainian].

30. Grigorchuk N.I. Broadening of surface plasmon resonance line in spheroidal metallic nanoparticles. *Journal of Physical Studies.* 2016. **20**(1–2): 1701.

31. Grygorchuk N.I. Behaviour of a line of the surface plasmon resonance in metal nanoparticles. *Metallofizika i Noveishie Tekhnologii.* 2016. **38**(6): 717.

32. Korotun A.V., Koval A.O., Reva V.I. Optical absorption of composite with bilayer nanoparticles. *Journal of Physical Studies.* 2019. **23**(2): 2603.

33. Korotun A.V., Koval' A.A. Optical Properties of Spherical Metal Nanoparticles Coated with an Oxide Layer. *Opt. Spectrosc.* 2019. **127**(6): 1161.

34. Korotun A.V., Koval' A.A., Reva V.I., Titov I.N. Optical Absorption of a Composite Based on Bimetallic Nanoparticles. Classical Approach. *Phys. Met. Metall.* 2019. **120**(11): 1040.

35. Korotun A.V., Karandas Ya.V., Reva V.I., Titov I.M. Polarizability of two-layer metal-oxide nanowires. *Ukr. J. Phys.* 2021. **66**(10): 908.

36. Korotun A.V., Karandas Ya.V. Surface Plasmons in a Nanotube with a Finite-Thickness Wall. *Phys. Met. Metall.* 2022. **123**(1): 7.

37. Korotun A.V., Pavlishche N.I. Anisotropy of the Optical Properties of Metal Nanodisks. *Opt. Spectrosc*. 2022. **130**(4): 269.

38. Liu M., Guyot-Sionnest P. Synthesis and Optical Characterization of Au/Ag Core/Shell Nanorods. *J. Phys. Chem. B.* 2004. **108**(19): 5882.

39. Constantin D. Why the aspect ratio? Shape equivalence for the extinction spectra of gold nanoparticles. *Eur. Phys. J. E.* 2015. **38**: 116.

40. Farokhnezhad M., Esmaeilzadeh M. Optical and Photothermal Properties of Graphene Coated Au–Ag Hollow Nanoshells: A Modeling for Efficient Photothermal Therapy. *J. Phys. Chem. C.* 2019. **123**(47): 28907.

41. Gans R. Über die Form ultramikroskopischer Goldteilchen. *Ann. Phys*. 1912. **342**(5): 881.

42. Link S., El-Sayed M.A. Shape and size dependence of radiative, non-radiative and photothermal properties of gold nanocrystals. *Int. Rev. Phys. Chem.* 2000. **19**(3): 409.